

Well tie for broadband seismic data

Ehsan Zabihi Naeini^{1*}, James Gunning² and Roy White³

¹Ikon Science - R&D, Causeway House, The Causeway, Teddington, London TW11 0JR, United Kingdom of Great Britain and Northern Ireland, ²CSIRO Petroleum, Ian Wark Laboratory, Bayview Ave, Clayton, Victoria 3168, Australia, and ³Birkbeck, University of London, 27 Kings Road, Walton on Thames KT12 2RA, United Kingdom of Great Britain and Northern Ireland

Received November 2015, revision accepted June 2016

ABSTRACT

The seismic industry is increasingly acquiring broadband data in order to reap the benefits of extra low- and high-frequency contents. At the low end, as the sharp low-cut decay gets closer to zero frequency, it becomes harder for a well tie to estimate the low-frequency response correctly. The fundamental difficulty is that well logs are too short to allow accurate estimation of the long-period content of the data. Three distinctive techniques, namely parametric constant phase, frequency-domain least squares with multi-tapering, and Bayesian time domain with broadband priors, are introduced in this paper to provide a robust solution to the wavelet estimation problem for broadband seismic data. Each of these techniques has a different mathematical foundation that would enable one to explore a wide range of solutions that could be used on a case-by-case basis depending on the problem at hand. A case study from the North West Shelf Australia is used to analyse the performance of the proposed techniques. Cross-validation is proposed as a robust quality control measure for evaluating well-tie applications. It is observed that when the seismic data are carefully processed, then the constant phase approach would likely offer a good solution. The frequency-domain method does not assume a constant phase. This flexibility makes it prone to over-fitting when the phase is approximately constant. Broadband priors for the time-domain least-squares method are found to perform well in defining low-frequency side lobes to the wavelet.

Key words: well tie, wavelet, broadband seismic, inversion.

1 INTRODUCTION

The volumes of broadband seismic data acquired and processed by the industry have grown rapidly. The spectral content of this new quality seismic data is demonstrably superior to conventional seismic data, both at the low and high frequency ends of the spectrum. Although this technology development started as an acquisition or processing dominated phenomenon, there is also increasing emphasis on benefits for quantitative interpretation (Reiser, Bird, and Whaley 2015; Zabihi Naeini 2014). It is our understanding that the general preference of seismic interpreters is to always use broadband seismic data, unless there is a good reason not to. The motive is

rather clear: by extending the low-frequency content, seismic amplitude inversion, which is the building block of quantitative interpretation, depends less on the background model, the construction of which is still a subject of ongoing research. An example is a recent approach to use the seismic image to guide the interpolation of well-log data to build background models (Zabihi Naeini and Hale 2015). Full-waveform inversion is another important application that demands more low frequencies (Baeten *et al.* 2013).

One could argue that the bottleneck for achieving a satisfactory quantitative interpretation and subsequently reservoir parameter estimation is the well tie, a process through which the seismic wavelet is estimated (Walden and White 1998; Nielsen, Klem, and Cherrett 2015). The principles of making a well tie are essentially the principles of system identification

*E-mail: enaeini@ikonscience.com

adapted to the characteristic properties of seismic data and well-log synthetic seismograms. It is not our intention to repeat these principles again, so we refer to a tutorial by White and Simm (2003) that covers them in more detail. However, broadband seismic data pose a challenge for well ties as the duration of the well log is often inadequate to estimate the low-frequency decay towards zero frequency (White and Zabihi Naeini 2014).

The difficulty in estimating the low-frequency decay towards zero frequency from a well tie originates in the limited duration T of log data available for a well tie. The reciprocal ($1/T$) of this duration limits the spectral resolution available from making the tie. Since often only a short log length is available, this introduces a severe limitation (~ 2 Hz for 500-ms log) in estimating a cut-off whose corner frequency may be as low as 2 Hz. In practice, spectral estimates made using this resolution will be very erratic, and some form of averaging is needed to stabilise the estimates. The actual resolution is defined by the analysis bandwidth b introduced below, where b is some small multiple of ($1/T$), and the product bT is an averaging factor equal to the number of independent spectral estimates entering the average. For a single well tie, the only available means of averaging is over adjacent frequencies, which renders it impossible to measure a 2-Hz cut-off frequency. Further, there is a tradeoff between: (i) the use of a small analysis bandwidth to avoid over-smoothing the spectrum; and (ii) the need for a reasonable amount of averaging in order to reduce estimation errors. To measure a low-frequency decay from a well tie will inevitably produce an unstable wavelet. There is no simple formula for selecting an appropriate analysis bandwidth since it depends on the structure of the wavelet's spectrum and the noisiness of the data as well as on T . Fortunately, the minimum in the root-mean-square wavelet error is fairly flat, and it is not difficult to select a suitable analysis bandwidth (White 1984, Fig. 11). By comparison, the estimation of the power spectrum of the seismic data is comparatively straightforward, is not limited by the log length, and can be enhanced by use of larger volumes of data.

The low-frequency decay of the amplitude spectrum is not the only issue; direct estimation of the low-frequency phase is also almost impossible. White and Zabihi Naeini (2014) proposed a practical solution to this problem that effectively consisted of: (i) estimating the wavelet using the available log length; (ii) using multi-taper spectral analysis of the seismic data over a long time window in order to estimate and modify the low-frequency decay of the estimated wavelet accordingly; and (iii) according to either the measured decay, or based on

the processing and acquisition information, modify the low-frequency phase (see, for details, White and Zabihi Naeini 2014, 2015).

Although the proposed approach above was a good start, it did not capture all of the possibilities and was very much a frequency-domain solution. Like many other applications, the well tie technique has to be adapted to the problem at hand, and the challenge with broadband seismic data is to find suitable ways around the lack of very long well logs. This implies that there is not necessarily only one way to carry out a well tie and that a variety of approaches has to be tested. In what follows, we introduce three different algorithms: parametric constant phase, modified least squares in the frequency domain (Walden and White 1998) with multi-tapering, and modified least squares in the time domain using a Bayesian approach (Gunning and Glinsky 2006) with broadband priors. As described later, these techniques have different mathematical foundations but share a common characteristic: a robust solution with a better handle on the low-frequency content.

It is worth mentioning that, although broadband seismic data also boost the high-frequency content, the resulting impact on the well tie is more tractable. This is because the main cause of error at high frequencies is the misalignment of the seismic data and the well-log synthetic. Therefore, to minimize the error on the high-frequency content, one requires precise timing of the well-log synthetic and more kinematically precise imaging (i.e., more accurate seismic velocities).

2 WAVELET ESTIMATION METHODS

2.1 Parametric constant phase

As mentioned above, direct and accurate estimation of the low-frequency phase is not possible from the well tie. A pragmatic approach is to use a constant phase approximation over the entire seismic bandwidth. This uses fewer degrees of freedom than estimating a phase spectrum and has some empirical basis in that, after processing, the phase of seismic wavelets is often approximately constant across the seismic bandwidth. When only a short log length is available, this approach is particularly suitable as, in practice, allowing the phase to vary with frequency could be unreliable in such cases. If required, one can modify the phase at the low frequencies towards zero frequency using the approach proposed by White and Zabihi Naeini (2014). In what follows, we describe our method of obtaining a constant phase wavelet by turning to the use of a long time window, many traces, and multi-taper spectral smoothing to estimate the low-frequency decay of the amplitude

spectrum. We also discuss how to compute other parameters such as lag and scale of the wavelet using the cross-covariance estimates.

2.1.1 Amplitude spectrum

As for the wavelet amplitude spectrum, we use

$$|W(f)| = \sqrt{\frac{P_s(f)}{P_r(f) + c}}, \quad (1)$$

where $P_s(f)$ is the seismic power spectrum, $P_r(f)$ is the reflectivity power spectrum, and c is a small whitening constant (i.e., a small percentage of the maximum reflectivity amplitude) for stabilisation.

Equation (1) obviously exhibits the need to compute power spectra. A standard method of power spectral analysis of a time series, such as a segment of seismic data, is to compute the auto-correlation of the data segment, apply a taper (lag window) to the auto-correlation, and Fourier transform the tapered auto-correlation. An alternative approach simply Fourier transforms the data segment and divides the squared amplitude spectrum by the segment length to form the periodogram; the periodogram is then smoothed with a spectral window. The results are equivalent if the spectral window is the Fourier transform of the lag window. The purpose of the spectral smoothing is to reveal the underlying shape of the spectrum of the data by reducing the sampling errors that impart a very ragged appearance to the periodogram. The lag window performs the same role by down-weighting and excluding the random fluctuations of the auto-correlation at longer lags.

An important property of a lag window is the analysis bandwidth, or equivalent statistical bandwidth, b of its spectral window, which is the effective bandwidth over which the spectrum is smoothed (White 1984), and such smoothing results inevitably in bias. In fact, in power spectral analysis, two types of bias should be considered: smoothing bias and leakage bias. The former is a result of smoothing, and the latter is a consequence of power leakage through the side lobes of the spectral window from the nearby passband. The Papoulis taper was designed to minimise the smoothing bias (Papoulis 1973). However, at low frequencies, it is important to minimise the spectral leakage too. Multi-taper spectral analysis, proposed by Thomson (1982), is designed for this task. It applies a set of orthogonal tapers to the data segment and averages their periodograms. Thomson's tapers are discrete prolate spheroidal sequences. We found that for seismic spectra the orthogonal tapers of Riedel and Sidorenko (1995)

perform better, with good protection against bias and leakage simultaneously. We use these tapers throughout this paper. An important factor to consider for multi-tapering is the number of tapers. According to Riedel and Sidorenko (1995), the first n ($n=2Tw-1$) tapers are concentrated in the band $[-w, w]$, where T is the window length, and w is the half-bandwidth. Thus $2w$ has a role similar to that of analysis bandwidth b for lag windows (the nearest integer can be selected for non-integer values). For example, if we have 1 s of data (T) and the desired half-bandwidth is 2 Hz (w), then it is recommended to use three tapers. We follow this rule when multi-tapers are used.

The Papoulis window is not ideal for measuring $P_s(f)$ because it introduces leakage from the seismic bandwidth below or above any sharp frequency cut-off. Pre-whitening filters are also generally incapable of compensating the low-frequency cut-offs considered here. Any pre-filter design, whether from correlations or spectra, would not see the sharp cut-off that is blurred by the truncation of its input data segments. Multi-taper spectral analysis is specially designed to minimise spectral leakage for data that have large variations in power between nearby frequencies. Our proposed strategy is therefore to compute $P_s(f)$ in equation (1) using multi-tapering over a long window and average over many traces around the well. The combined effect of multi-tapering, long time window, and averaging yields $P_s(f)$ with a much finer resolution (compared with that of $P_r(f)$), giving a better chance of estimating the low-frequency cut-off. The averaging also helps to stabilise the spectral estimates by smoothing over small-scale minor fluctuations.

To compute $P_r(f)$, we can only use whatever window length the logs allow. However, reflectivity spectra are generally considered fairly smooth, generally increasing in power from low to high frequencies, thereby producing a so-called blue colouring. Consequently, their estimation does not need a high-resolution method, and the tapered auto-correlation method (e.g., Papoulis 1973) is well suited to producing a smooth spectrum. The blue character of the well-log reflectivity would have minimal effect on the amplitude spectrum of the wavelet at the very low frequencies.

2.1.2 Phase spectrum, time lag, and scale factor

The estimation of phase and time difference is a key part of seismic data analysis and also, more generally, in other signal processing applications. As far as the subject of this paper is concerned, the phase and time difference are determined by tying synthetic seismograms to real seismic data at well

locations. In the examples shown later, the synthetic seismograms were constructed from calibrated sonic logs that consequently determined their timing. No attempt was made to adjust the timing in order to improve the fit to the seismic data. When there is no check shot or vertical seismic profile data available to calibrate the sonic log, or it comes from a deviated well, the use of the well tie to determine or tune the time–depth relation needs to be tightly constrained in order to avoid any possibility of forcing a fit or, in the case of a long well log, of confusing the time–depth relation with time variation of the seismic wavelet.

Apart from timing and phase, and to complete the well-tie story, a scale factor is also needed so that when the scaled wavelet is convolved with the reflectivity, it generates a synthetic seismogram that matches the amplitudes of the seismic data.

The main requirement on the accuracy of these estimates is that they should have minimum error, whether random or systematic (bias). The principle of maximum likelihood (Brandt 1976) yields estimates that asymptotically have minimum variance and are unbiased. Simulations demonstrate that, for data having a fairly uniform signal-to-noise ratio (S/N) across their frequency bandwidth, the accuracy of phase and time shifts estimated as follows is close to the Cramer–Rao bound, i.e., the limiting accuracy of maximum-likelihood estimates (Brandt 1976). Let $\phi_{sr,\tau}$ be the cross-correlation of the seismic s and synthetic r , and $\psi_{sr,\tau} = HT[\phi_{sr,\tau}]$ be the Hilbert transform of the cross-correlation. Then, the envelope of the cross-correlation is

$$A_{sr,\tau} = \sqrt{\phi_{sr,\tau}^2 + \psi_{sr,\tau}^2}, \quad (2)$$

and its instantaneous phase is

$$\theta_{sr,\tau} = \tan^{-1} \left(\frac{\psi_{sr,\tau}}{\phi_{sr,\tau}} \right). \quad (3)$$

The envelope peak is $\max(A_{sr,\tau})$. The time of the envelope peak estimates the time difference between the signals on the two recordings, and the instantaneous phase $\theta_{sr,\tau}$ at the envelope peak estimates the phase shift between them. These can be incorporated into the seismic wavelet as time and phase shift values. Furthermore, a least-squares scale factor can be computed as the magnitude of the envelope peak divided by the peak of the auto-correlation of the synthetic seismogram.

White and Simm (2003) emphasise the importance of measuring the accuracy of the wavelet as well as goodness-of-fit when tying synthetic seismogram to real seismic data. Hamon and Hannon (1974) give a general equation for the

variance–covariance matrix of the maximum-likelihood phase estimates from a parametric phase model. For a phase model of the form $2\pi f\tau + \theta$ consisting of a constant time shift and constant phase angle and assuming a fairly constant S/N over the seismic bandwidth, we derive the following expressions for the variances of time shift τ and phase θ :

$$\text{variance}\{\tau\} = \frac{3}{\pi^2 B^2} \frac{(R^{-2} - 1)}{2BT}, \quad (4)$$

$$\text{variance}\{\theta\} = \frac{(R^{-2} - 1)}{2BT}, \quad (5)$$

where R is the magnitude of the peak of the cross-correlation envelope (corresponding to spectral coherence), B is the seismic bandwidth, and T is the time window length. The standard errors in time shift and phase of the wavelet are therefore the square roots of the variances in equations (4) and (5) (see Appendix for the derivation of these equations). Interestingly, it is evident from these equations that the accuracy of the time and phase estimates depends on the bandwidth of the data. Despite the fact that broadband seismic data introduces some complexity at the low end of the spectrum, the extra bandwidth helps reduce the error in time and phase shift estimation.

2.2 Frequency-domain least squares

A routine least-squares best-fit well tie assumes that the synthetic seismogram is error free. As a consequence, the best-fit filter is not the seismic wavelet but the wavelet combined with a Wiener filter for attenuating the noise in the synthetic. The frequency-domain solution can be adapted to account for errors in the synthetic seismogram as well as noise in the data (Walden and White 1998). The frequency-domain approach also has the major advantage of providing diagnostics of the accuracy of a well tie, such as error bars or confidence bounds on the amplitude and phase spectrum of the seismic wavelet (in fact, equations (4) and (5) can be interpreted as a special case of frequency independent variances). We refer to White (1980) and Walden and White (1998) for a comprehensive review of the frequency-domain least-squares technique.

However, the basic requirement of the frequency-domain least-squares solution is to compute the auto- and cross-spectra. As mentioned in the previous section, the auto- and cross-spectra can be computed as Fourier transforms of auto- and cross-correlations or by auto- and cross-products of the Fourier-transformed data segments.

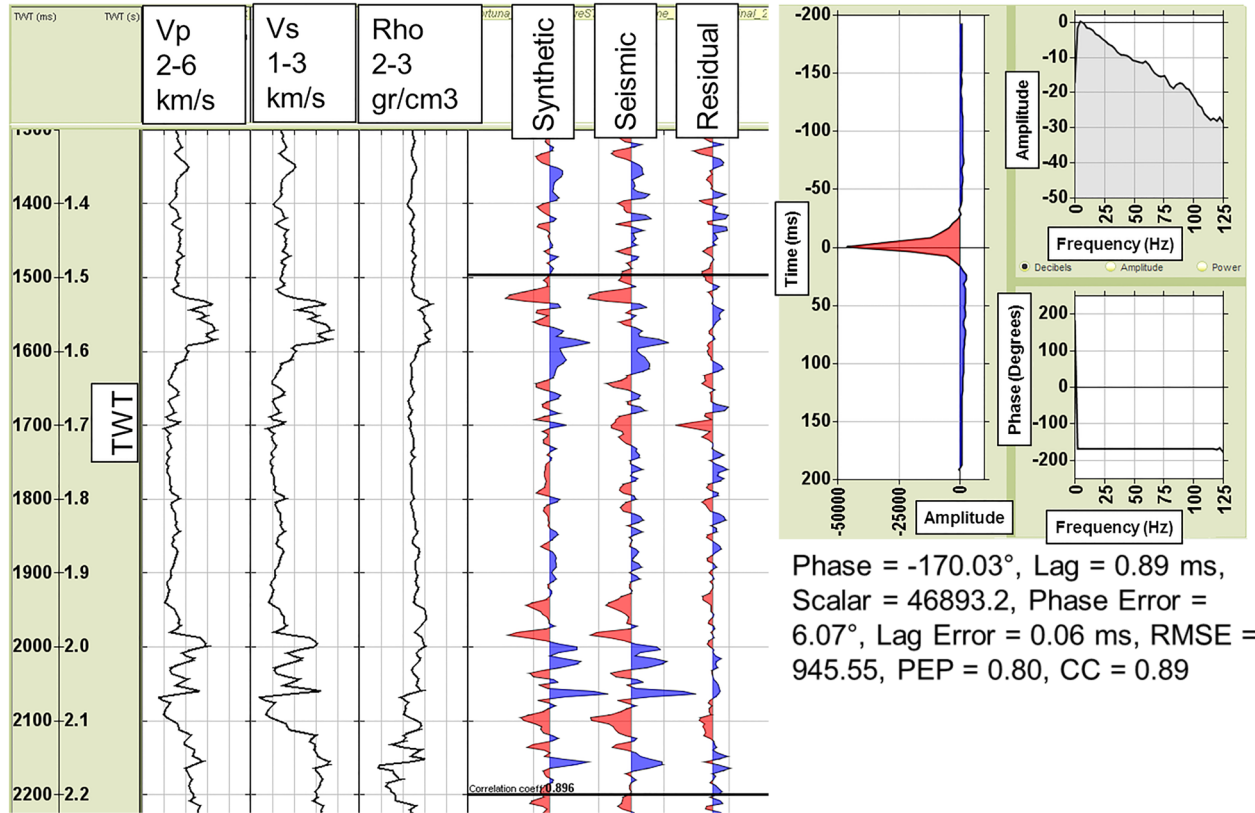


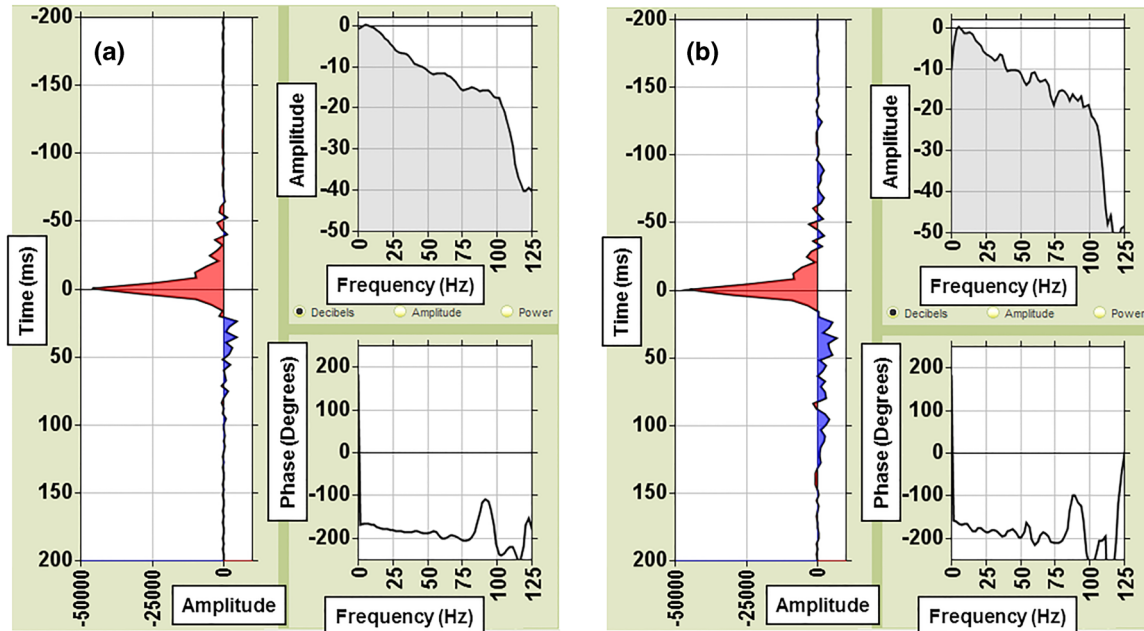
Figure 1 Well-tie plot at well 1 from using a constant phase wavelet. The well tie QC attributes are also shown. Overall, this figure shows a very high quality well tie.

Our proposed method here is to use exactly the same algorithm as in Walden and White (1998), but we modify the auto- and cross-spectra calculation. While traditionally Papoulis tapers (Papoulis 1973) are used to taper the auto- and cross-correlation estimates and then to Fourier transform, we propose the use of multi-tapering on data segments, Fourier transform, and then compute the auto- and cross-spectra. The advantage of using multi-tapers has already been described in the previous section (i.e., to reduce the smoothing and leakage bias) and here again we use tapers of Riedel and Sidorenko (1995).

2.3 Time-domain Bayesian least squares

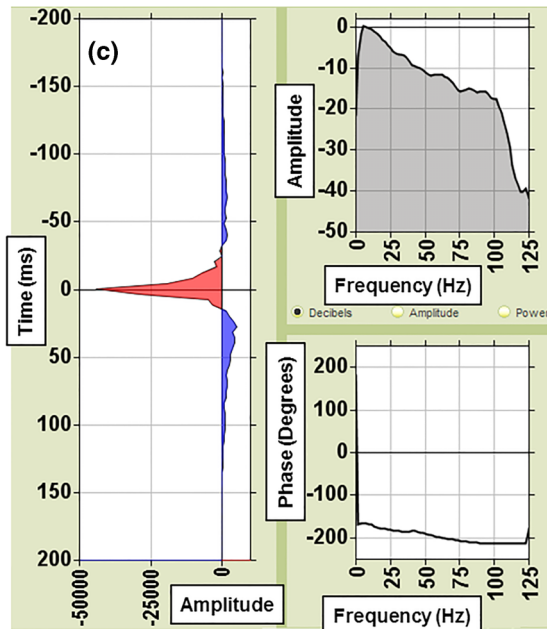
Gunning and Glinsky (2006) introduced a well-tie algorithm formulated in the time domain as a Bayesian inverse problem. The algorithm simultaneously estimates all the wavelet coefficients, and the Bayesian formulation allows one to incorporate uncertainties associated in the time–depth mapping, positioning errors, and other useful priors. Similarly, the Bayesian approach provides tools for computation of full

posterior uncertainties of the model parameters. Gunning and Glinsky (2006) also discuss the problem of wavelet length, and treat this as a model dimension parameter that may be estimated via Bayesian model selection theory (Denison *et al.* 2002). The length is selected using the Bayesian model evidence and is closely connected to the Bayesian information criterion (BIC), which is a selection tool for choosing a model from among a set of candidate models (Denison *et al.* 2002). The model evidence combats overfitting by reducing the number of parameters in the model (in this case wavelet coefficients), and this is very effective at suppressing noise in the wavelet tails. The model evidence or BIC puts maximum posterior probability on the simplest model that adequately fits the data, thus behaving as a formal “Occam’s razor” (Denison *et al.* 2002), i.e., the preference for a simple model to a more complex one, other things being equal. We refer to Gunning and Glinsky (2006) for more details on this technique. In what follows, we introduce two functionality enhancements in the form of priors that are specifically targeted to handle the low-frequency character of the wavelet in this algorithm.



Phase intercept = -169.36° , Lag = 0.0, max amplitude = 45834.81, Phase Error = 7.07° , RMSE = 949.39, PEP = 0.80, CC = 0.89

Phase intercept = -170.15° , Lag = 0.0, max amplitude = 44493.96, Phase Error = 6.43° , RMSE = 884.64, PEP = 0.82, CC = 0.91



RMSE = 949.14, PEP = 0.80, CC = 0.89

Figure 2 Wavelets estimated using the frequency-domain least-squares method at well 1 with (a) Papoulis tapering, (b) multi-tapering, and (c) Papoulis modified by imposing the low-frequency amplitude decay of multi-taper wavelet and removing the unrealistic kink in the phase spectrum at around 80 Hz.

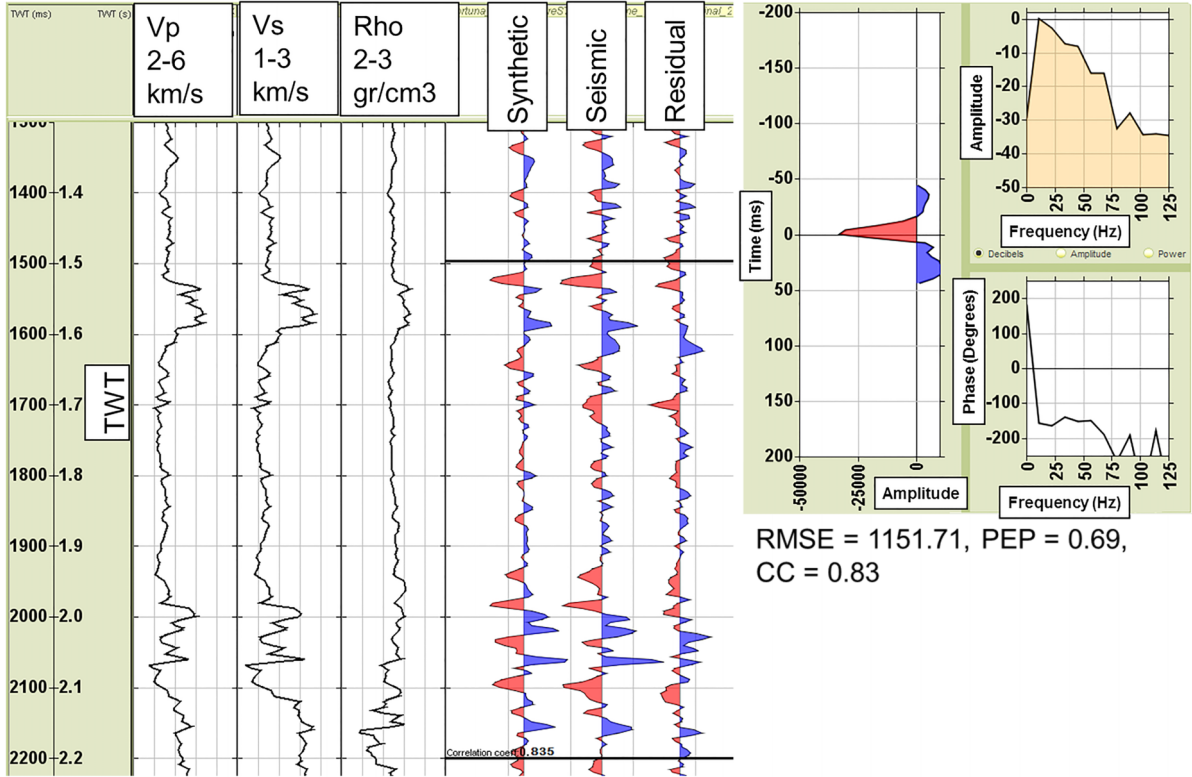


Figure 3 Well-tie plot at well 1 from Bayesian time-domain least-squares with auto-selection of the wavelet length.

2.3.1 Low-order polynomial decay

At very low frequencies, the log and hence the reflectivity data do not have much influence on the wavelet spectrum because of their blue (i.e., weakening) spectral character. The wavelet's low-frequency character is therefore most likely dominated by the seismic data. The latter is a consequence of the low cut of the instrumental response and any subsequent signature removal, zero phasing, Wiener shaping (e.g., shaping to a band-limited zero-phase pulse), and Q-treatment (to compensate absorption) that has occurred in the processing. This low-frequency decay eliminates all DC power and yields a low-order power-law decay for the wavelet spectrum of form $W(f) \sim f^{p+1}$, with possibly $p = 0$ or $p = 1$. This comes from a simple power expansion of the Fourier transform representation of $w(t)$,

$$\begin{aligned}
 W(f) &= \int_{-T}^T w(t) \exp(-2\pi i f t) dt \\
 &= \int_{-T}^T w(t) dt - 2\pi i f \int_{-T}^T t w(t) dt - 4\pi^2 f^2 \int_{-T}^T t^2 w(t) dt + \dots
 \end{aligned} \tag{6}$$

that facilitates the power-law decay to be implemented in the time domain as wavelet-coefficient constraints in the form of

$$\sum_{k=-N}^M a_{w,k} k^l = 0, \quad l = 0, \dots, p. \tag{7}$$

These confine the set of wavelets to a subspace of reduced dimensionality. Each l index in equation (7) represents an individual term in the right-hand side of equation (6), i.e., $p = 0$ suppresses the first term in equation (6), $p = 1$ the first two terms, and so on. Here, there are N wavelet coefficients before zero lag (i.e., negative lags), and M coefficients after zero lag (i.e., positive lags). For simplicity in implementation, these are imposed by remapping the Bayesian prior-precision matrix (inverse covariance) for the wavelet coefficients in $C_p = \text{diag}\{\sigma_w^2\}$ to $C_p^{-1} \rightarrow C_p^{-1} + \lambda^2 X_p^T X_p / \sigma_w^2$, where X_p is a matrix with rows representing the constraint equations [(7), above] ($X_{p,lk} = k^l$, $l = 0, 1, \dots, p$, $k = -N \dots M$), λ is a constant set just large enough to enforce the constraint tightly (but not perfectly), and σ_w is the prior uncertainty in the wavelet coefficients. This remapping confines the set of prior

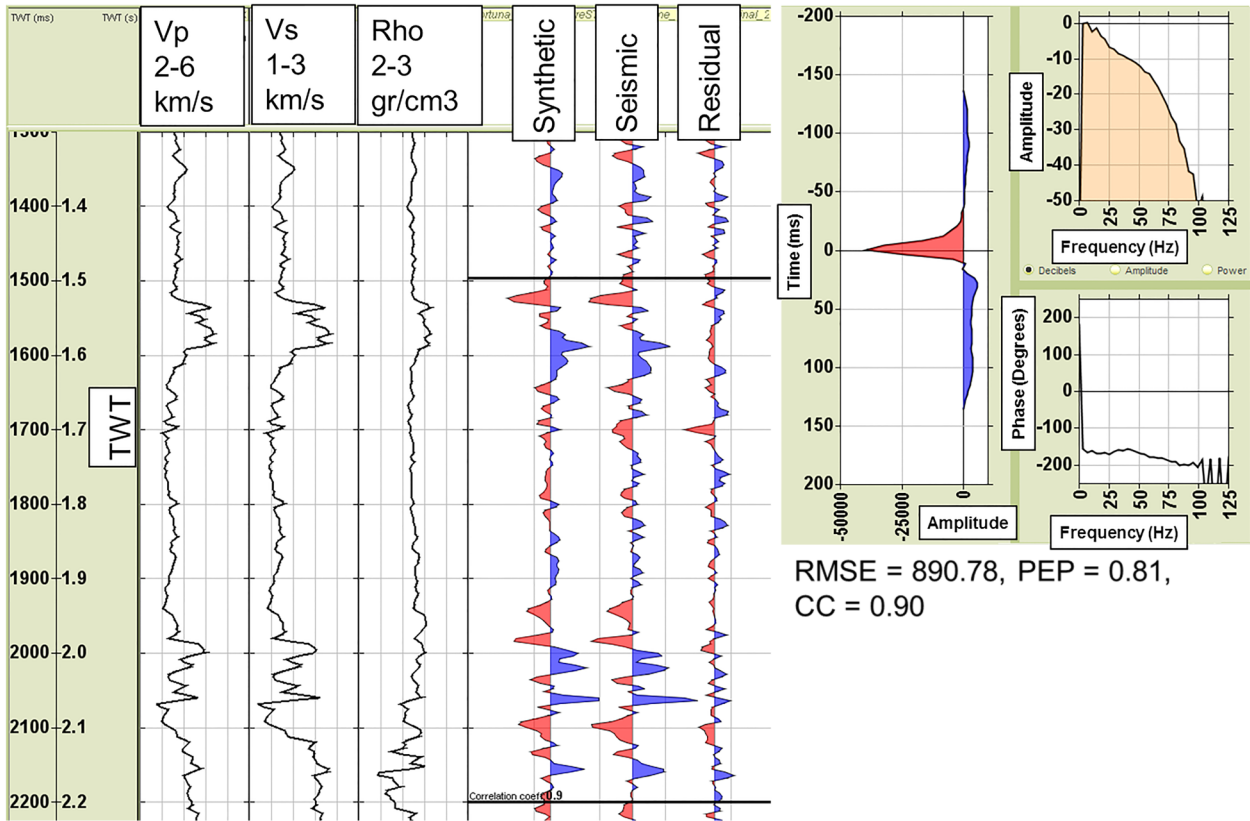


Figure 4 Well-tie plot at well 1 from Bayesian time-domain least squares with broadband priors.

models with appreciable probability to wavelets whose first p moments are zero.

2.3.2 Smooth wavelet tails

Broadband signatures observed in practice with a successful recovery of the low-frequency content have the character of appearing almost like a perfect spike, but with long, weak, and very smooth wavelet coefficients at larger positive and negative lags (e.g., wavelet side lobes). The long tails have a low-frequency character and, given the diminishing natural well log reflectivity power at low frequencies, they will contribute only rather modestly to synthetic amplitudes and any misfit improvement. Since they require numerous wavelet coefficients, the standard Bayesian evidence will strongly demote such models unless the new coefficients yield very significant misfit improvements, which is unlikely. Normally, wavelets estimated with long flexible tails tend to fill up with noise-related over-fitting features. Therefore, even if these weak tails are truly present underneath the spurious features, the anti-overfitting Occamist machinery tends to overwhelm them.

Roughly speaking, they demand too many degrees of freedom for marginal improvements in data fit, at least in sample-based representation.

The long tails may result from physical processes that are inherently slow but can be described with very few parameters, such as the tail decay of a Butterworth filter impulse response (ten Kroode *et al.* 2013), or perhaps residual artefacts of the slow air-bubble oscillations (Poole *et al.* 2013). So, a representation of these tails in a more parsimonious form may help them to survive the model-selection tests that usually favour shorter wavelets.

We propose a mode of inference wherein the wavelet coefficients a_w outside the interval $[-T, T]$ are strongly correlated and tapered. When this mode operates, the tail coefficients have their prior covariance set to the simple kriging covariance (Deutsch and Journel 1997) generated by the correlation structure $C_{p,i,j} \sim \sigma_w^2 \exp(-|i - j|/\lambda_T)$, with zero values at the wavelet edges, where p is as defined in equation (7), i and j are sample indexes, σ_w is the uncertainty in wavelet coefficients, and λ_T is the correlation length. The blocks of C_p corresponding to the positive lags $[T, T_{max}]$ do not

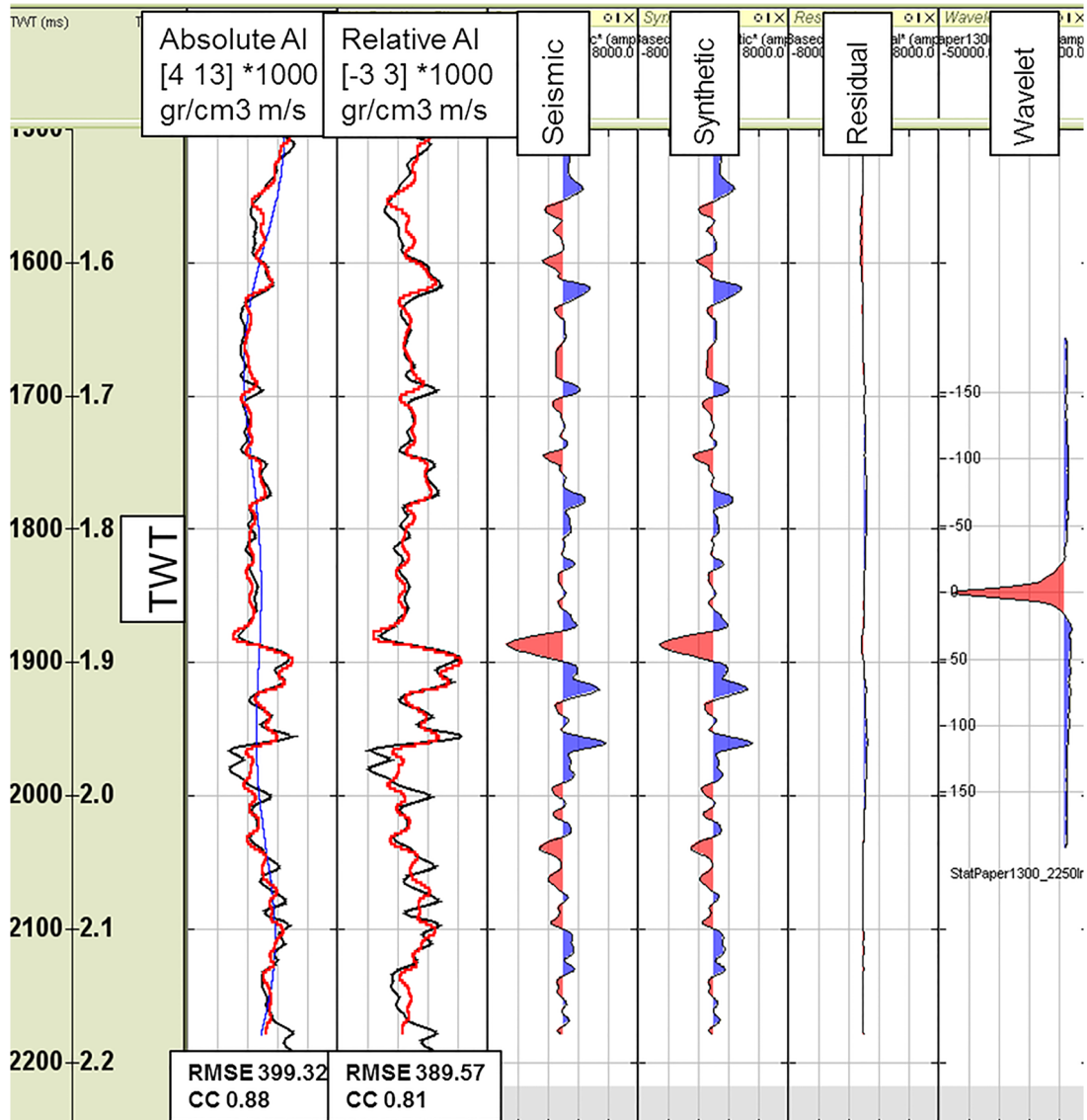


Figure 5 Blind QC at well 2 using the constant phase wavelet from well 1 (see also Fig. 1). The red curve is the inverted impedance, and the black curve is the well-log impedance.

correlate with the blocks of negative lags $[T_{min}, -T]$, and the central values are uncorrelated. The outcome of this technique is that the long tails are generated by many fewer effective degrees of freedom in the prior, and the model-selection machinery then begins to promote these longer models.

3 REAL DATA EXAMPLE

A broadband dataset from the North West Shelf of Australia has been used in this paper. The majority of the area is gently dipping, and we used two sub-cubes of data around two wells.

The seismic data are sampled at 4 ms, has a high signal-to-noise ratio, and also exhibits a very good bandwidth from 3 Hz to approximately 80 Hz, as will be seen in the estimated wavelets. In the following, we compare the performance of the wavelet estimation techniques introduced in this paper: constant phase, frequency-domain least squares with Papoulis and multi-tapering, and Bayesian time-domain least squares with and without broadband priors.

An important aspect of well tie is quality control (QC). One can use the estimated wavelets to invert the seismic data for impedance at the well location. However, by inverting at

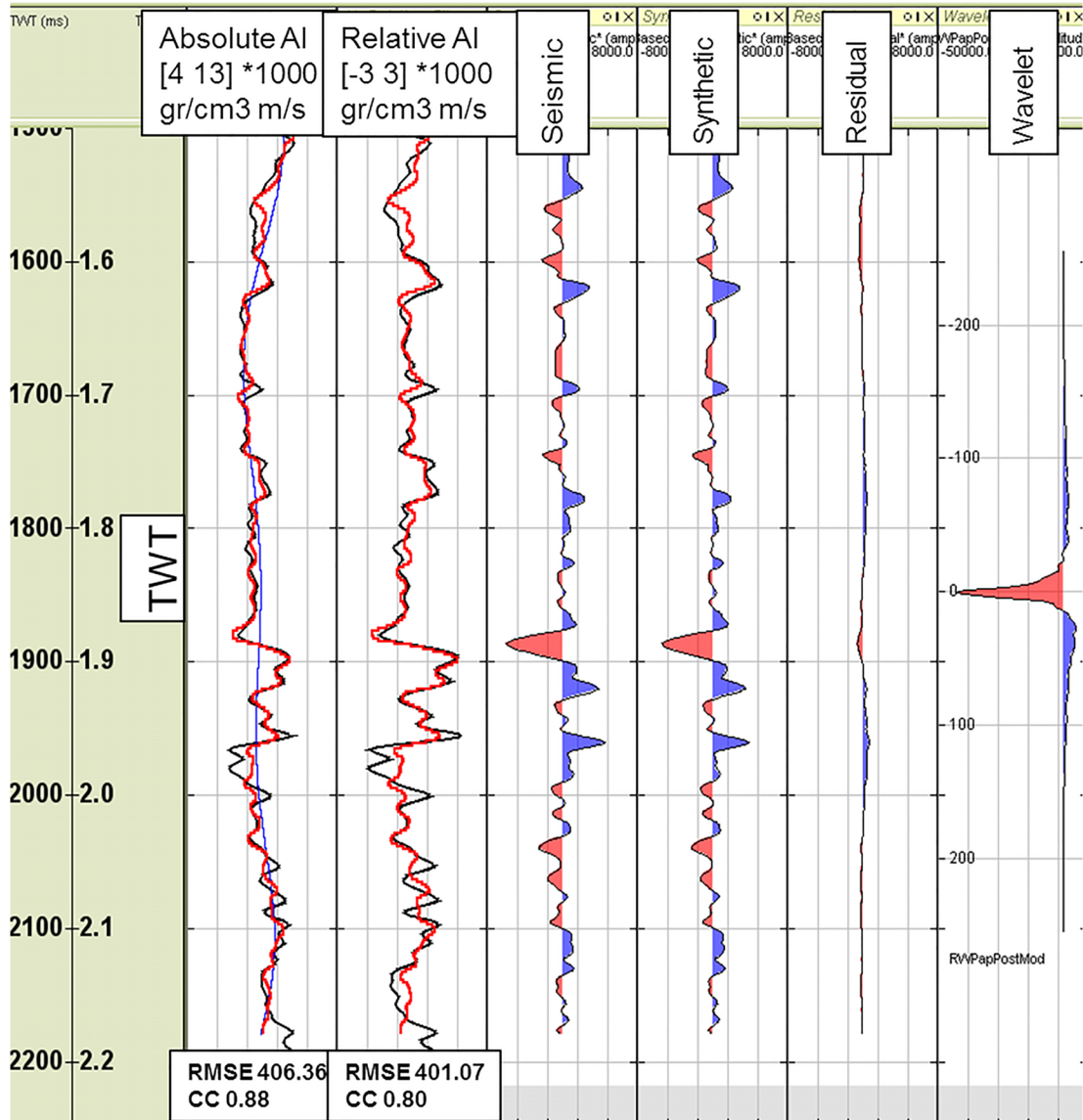


Figure 6 Blind QC at well 2 using the frequency-domain least-squares wavelet from well 1 (see also Fig. 2c). The red curve is the inverted impedance, and the black curve is the well-log impedance.

the same well, the estimated wavelet almost always leads to an acceptable result. A more rigorous and physically valid approach would be cross-validation, which would require at least two wells. Here, by having two wells, we have taken the cross-validation approach to analyse the quality of the well-tie wavelets. The input seismic data are the near-angle stack cube. To facilitate this, the wavelets estimated at well 1 are used in a model-based inversion engine to invert for acoustic impedance (AI) at well 2 and *vice versa* (this is also sometimes referred to as blind QC to signify that the QC is performed at a well that was not involved in the derivation of the wavelet).

Model-based inversion (or more generally simultaneous pre-stack inversion) is often formulated to minimise:

$$E = \|y - G\mathbf{m}\|^2 + \lambda\|\mathbf{m} - \mu\|^2, \tag{8}$$

where \mathbf{m} is the logarithm of impedance (the logarithm is imposed to linearise the inverse problem), μ is the low-frequency background model (Douma and Zabihi Naeini 2014), y is the seismic data, and G is the forward modelling matrix that includes the wavelet coefficients in a convolutional matrix form. The model weight λ quantifies the importance attached to the second term (model residual) relative to the first term (data

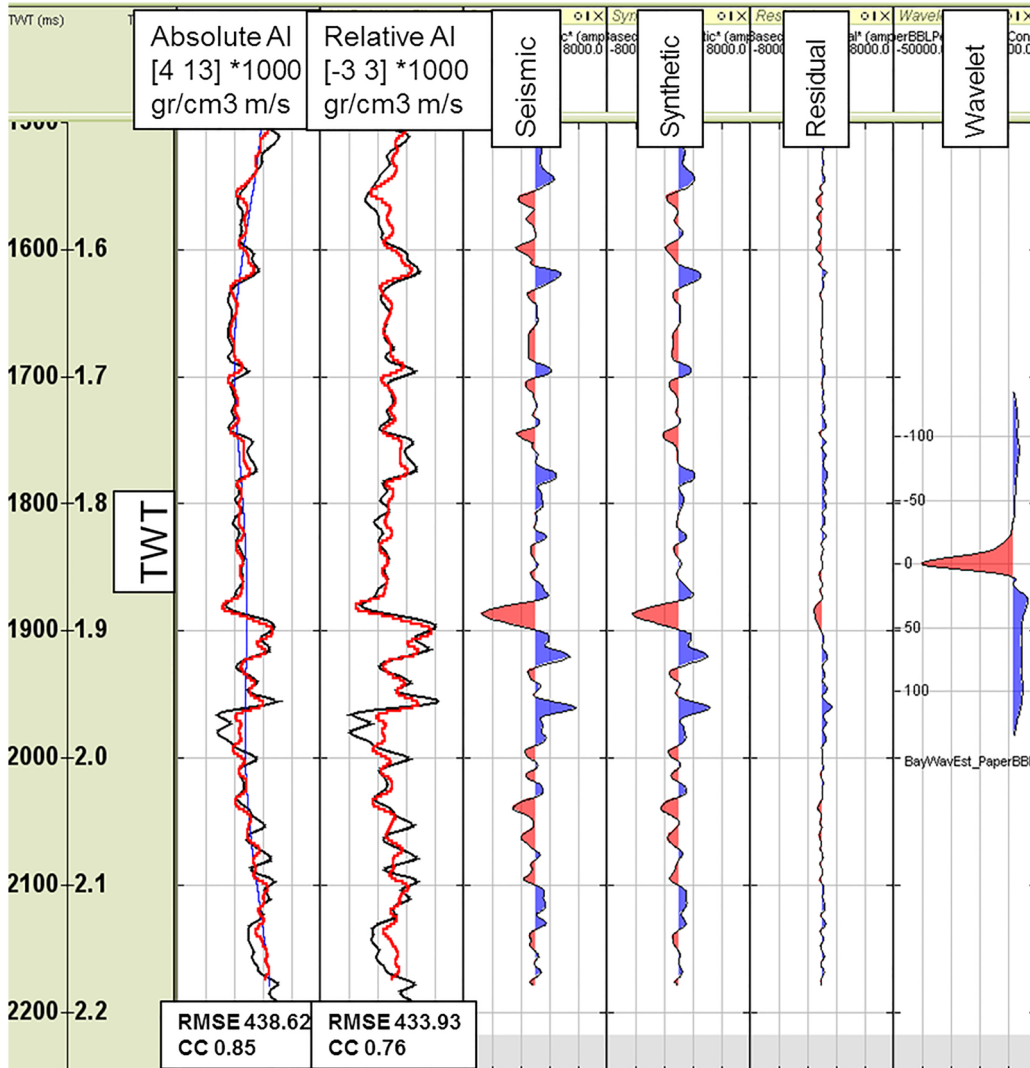


Figure 7 Blind QC at well 2 using the Bayesian time-domain least-squares wavelet with broadband priors from well 1 (see also Fig. 4). The red curve is the inverted impedance, and the black curve is the well-log impedance.

residual) in equation (8) and therefore is equivalent to the ratio $(\frac{\sigma_d}{\sigma_m})^2$ where σ_d is the noise root mean square (RMS), and σ_m is the standard deviation of the model. Here, σ_d can be estimated from the well-tie process (i.e., RMS of the error reported as RMSE in our well-tie plots) and should be incorporated accordingly in cross-validation tests. σ_m is estimated from well-log data deviations from the low frequency trend (σ_m does not change when the input wavelet changes).

3.1 Wavelet estimation at well 1 and QC at well 2

Figure 1 shows a well-tie plot at well 1, including the V_p , V_s , density (Rho) logs, the synthetic seismogram using the

estimated constant phase wavelet shown on the right, the recorded seismic data at the well, and the residual. The well tie is performed using the available log length of 900 ms, as shown in Fig. 1. Using equations (2) to (5), the estimated phase, lag, and the corresponding errors are also displayed. The amplitude spectrum of the wavelet demonstrates the broad bandwidth of the input seismic data. The low-frequency decay, which manifests itself in the long and smooth tails of the wavelet, indicates that our proposed strategy of using a long time window of the seismic data combined with multi-tapering works very well.

The correlation coefficient (CC), proportion of the energy predicted by synthetic seismogram (PEP, White and Simm

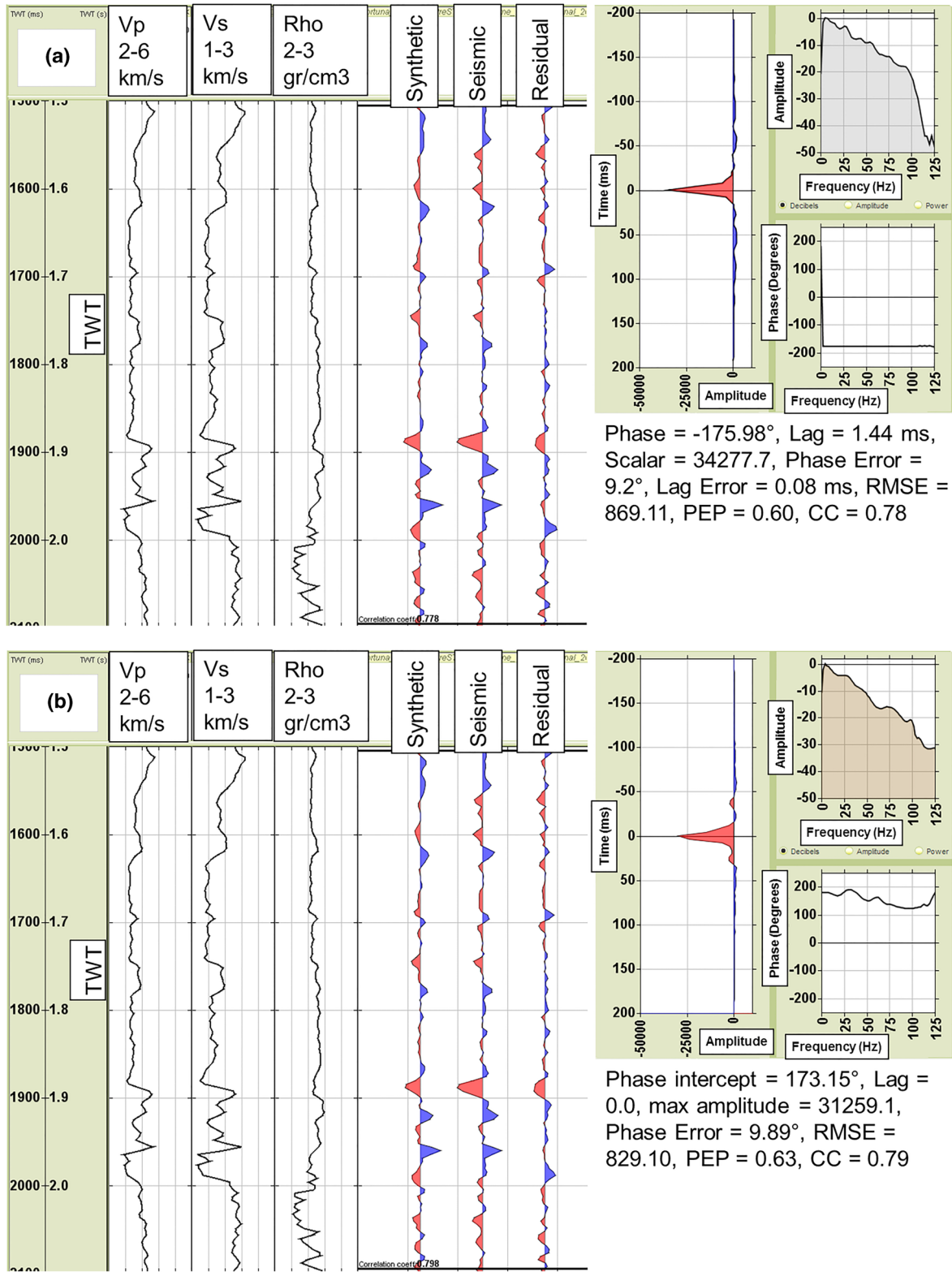


Figure 8 Well-tie plots at well 2 from (a) constant phase, (b) frequency-domain least squares with multi-taper modification, and (c) Bayesian time-domain least squares with broadband priors.

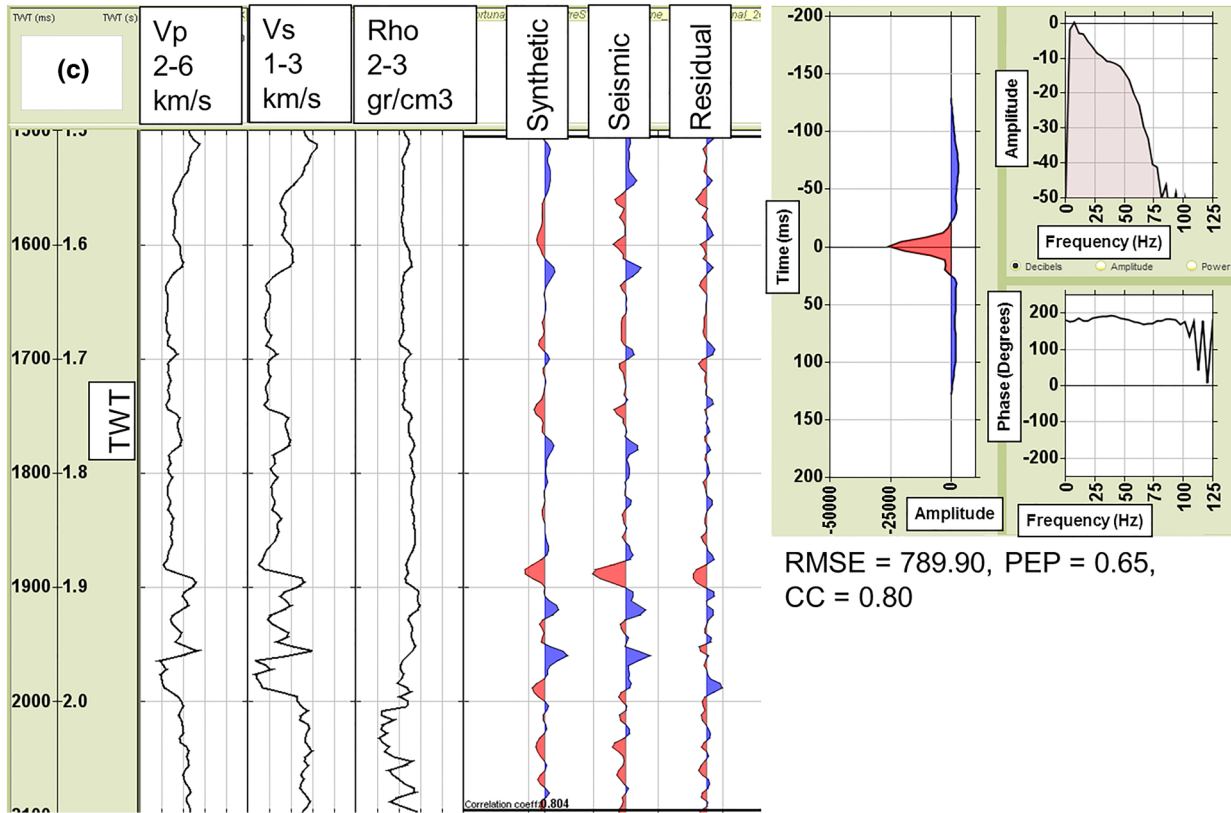


Figure 8 Continued

2003), and the RMSE of the data-synthetic misfit are also reported in Fig. 1. As can be observed, this wavelet results in a very good quality tie. RMSE will be used in impedance cross-validation QC later. In the following, to save space, we show the well-tie plots only when required. In other cases where there is not a significant difference visually, we only show the estimated wavelets.

Figure 2 shows two wavelets from the frequency-domain least-squares method. The wavelet in Fig. 2(a) is with Papoulis tapering and Fig. 2(b) is with multi-tapering. It is evident that the low-frequency decay is not captured when Papoulis tapering is used. Multi-tapering indicates a low-cut decay without estimating it well and at the cost of a slightly noisier spectrum. Moreover, the kink in the phase spectrum around 80 Hz (possibly due to low S/N) does not look realistic. One would ideally like to have a smooth spectrum similar to that of Papoulis but with a better decay. This can be achieved by imposing the low amplitude decay from the multi-taper wavelet on the Papoulis wavelet. Furthermore, the kink in the phase spectrum at 80 Hz can be smoothed. The final result is shown in Fig. 2(c), in which the wavelet, notably the side lobes which are an

important indicator of noise and over-fitting, now appears to be more stable and less noisy. It can be observed that the well-tie QC attributes (RMSE, PEP, and CC) do not change significantly with such modifications at the low end of the spectrum. This demonstrates the insensitivity of the well-tie process to the very low-frequency content. Nevertheless, these attributes show a high-quality well tie, and moreover, the outcome is consistent with the constant phase wavelet in Fig. 1. Further possibilities are to extrapolate the phase at low frequencies to a multiple of 90° at 0 Hz following White and Zabihi Naeini (2014). We have not observed any significant benefit of doing that on this dataset.

As mentioned, in the Bayesian time-domain least-squares method, Gunning and Glinsky (2006) discussed the problem of wavelet length and treated it as a model-selection problem. That is, they invert for the most likely wavelet model among N models with different lengths. Although their implementation is different, it is similar to the standard Bayesian information criterion (BIC), which effectively penalises models that fit only marginally better than simpler models (e.g., shorter wavelets). Figure 3 shows the

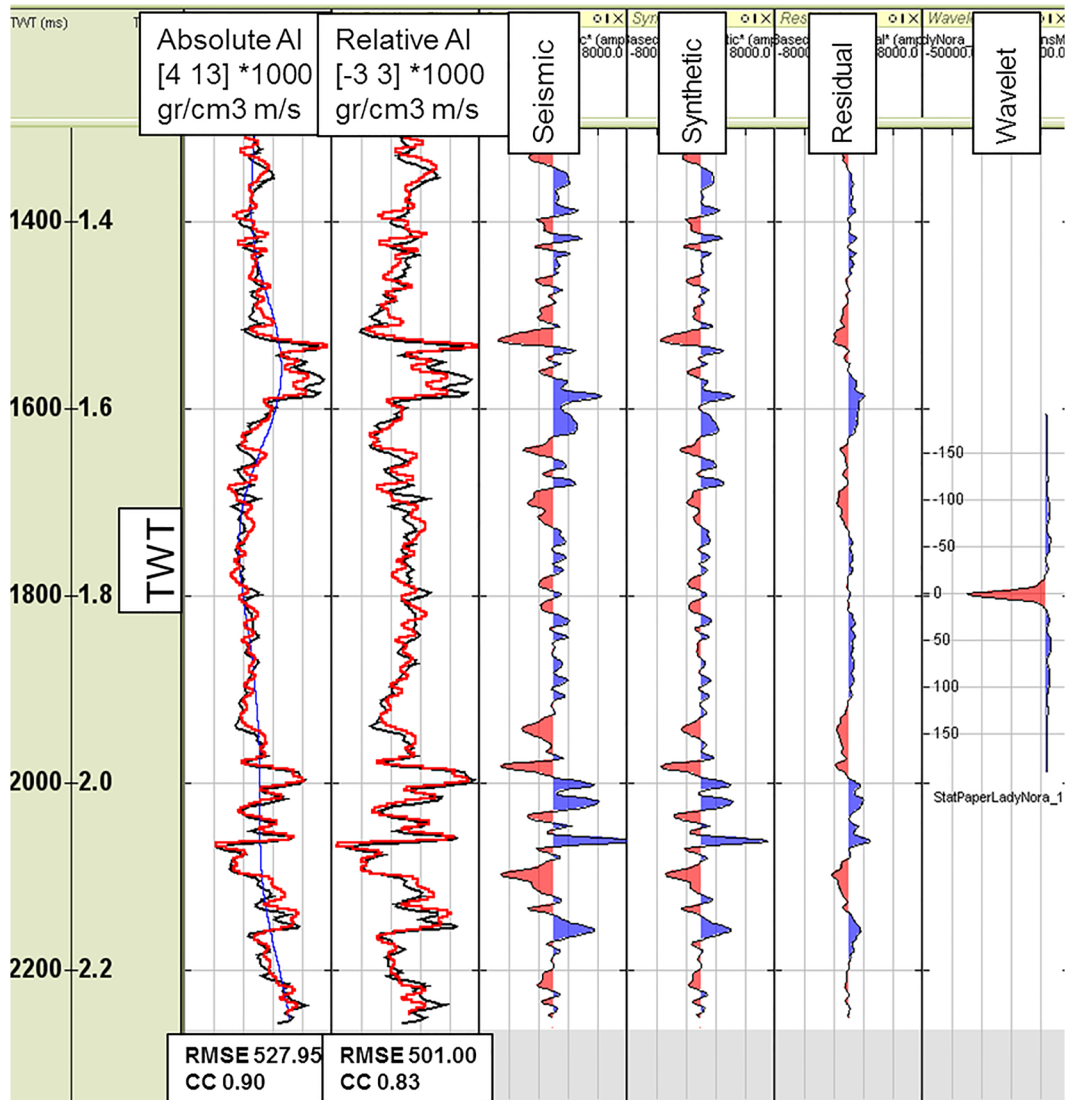


Figure 9 Blind QC at well 1 using the constant phase wavelet from well 2 (see also Fig. 8a). The red curve is the inverted impedance, and the black curve is the well-log impedance.

well-tie plot and the estimated wavelet with auto-selection of the wavelet length. The well tie produces a significantly shorter wavelet with more misfit energy than the previous two methods, and the resulting wavelet does not carry the low-frequency content expected from this dataset. Figure 3 is only shown here to demonstrate the need for broadband priors introduced in this paper for the time-domain least-squares method.

Figure 4 shows the well-tie plot from the same method but with a user-defined wavelet length and appropriate broadband priors as discussed. In this case, the first-order polynomial decay is set to zero, and wavelet tails are constrained to be

smooth. The estimated wavelet now is significantly improved and exhibits a sharp decay at low frequencies. RMSE (note also the reduction in residual), PEP, and CC are also improved when compared with those in Fig. 3. It is reassuring that all three methods result in a very good well tie and the estimated wavelets have similar characters.

The estimated wavelets in Figs. 1, 2(c), and 4 are now selected for QC at well 2. This is a completely blind QC, i.e., we use a model-based inversion to invert for AI at well 2 using the selected wavelets estimated at well 1. The results are shown in Figs. 5, 6, and 7. The RMSE between the inverted relative impedance and well-log relative impedance is a very useful QC

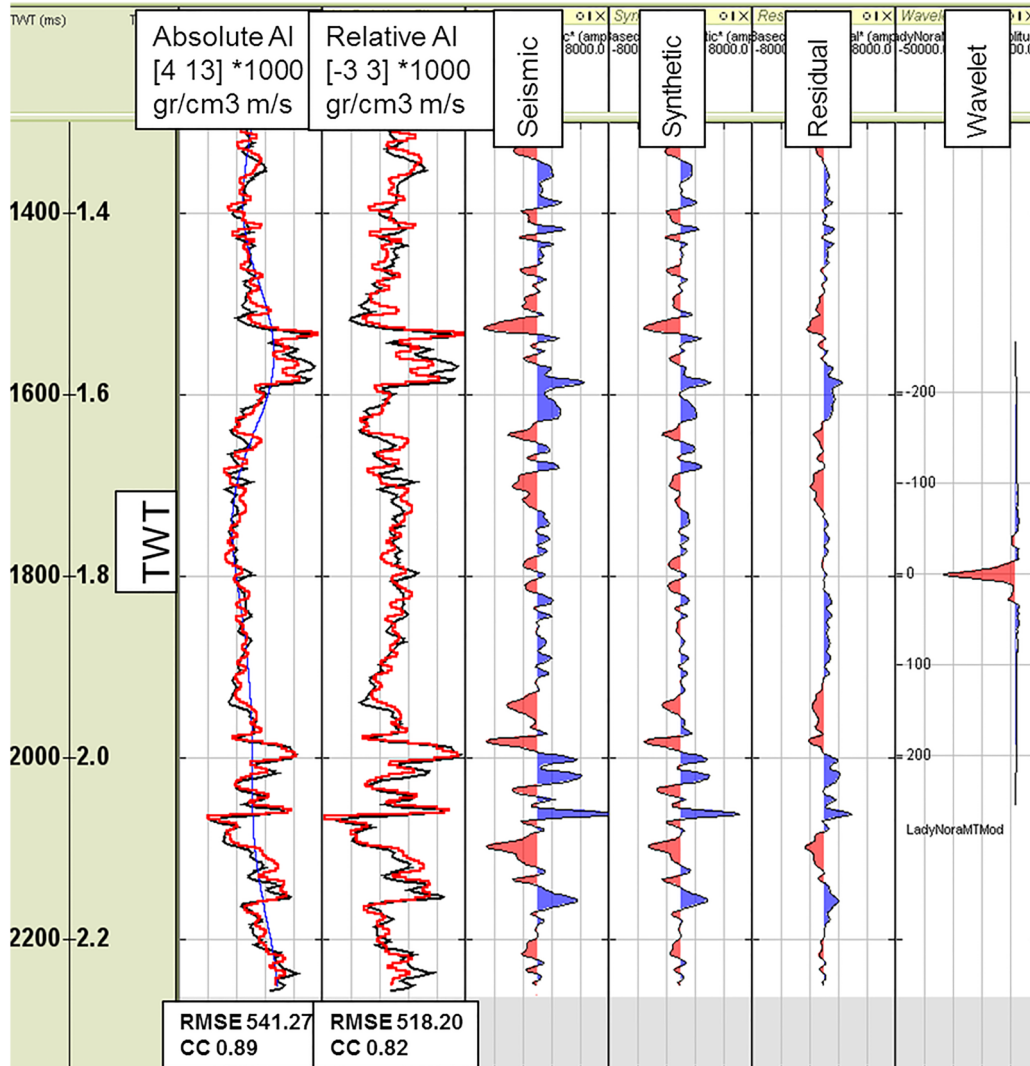


Figure 10 Blind QC at well 1 using the frequency-domain least-squares wavelet with multi-taper modifications from well 2 (see also Fig. 8b). The red curve is the inverted impedance, and the black curve is the well-log impedance.

tool. CC is also displayed for reference. Generally, we prefer to analyse the RMSE and CC of the relative impedance as the CC for the absolute impedance is biased by the impact of the low-frequency background model (shown by a thin blue curve in the absolute impedance panel). The difference between the real seismic data and the modelled synthetic (residual panel in Figs. 5, 6, and 7) is also a useful attribute. The very low amplitudes of the residual traces from the inversion compared with those from the well ties show that the inversion drives misfit errors into the inverted impedance. Nonetheless, the residual traces are helpful in that they indicate any mismatch in the low-frequency content (Figs. 6, 1.8–2 s) or in high-frequency content (Fig. 7). These effects are seen better

in section displays (White and Zabihi Naeini 2014). It can be observed that all wavelets produce impedance that fits the well-log impedance almost equally well. The constant phase wavelet has the lowest RMSE of the relative impedance, and the residuals between the seismic data and synthetic traces are the smallest of the three.

3.2 Wavelet estimation at well 2 and QC at well 1

Well-tie experiments are performed in the same order as in the previous section to complete the cross-validation. Well 2 has 600 ms of log data available; therefore, we expect well-tie quality to be lower. The estimated wavelets at this well are

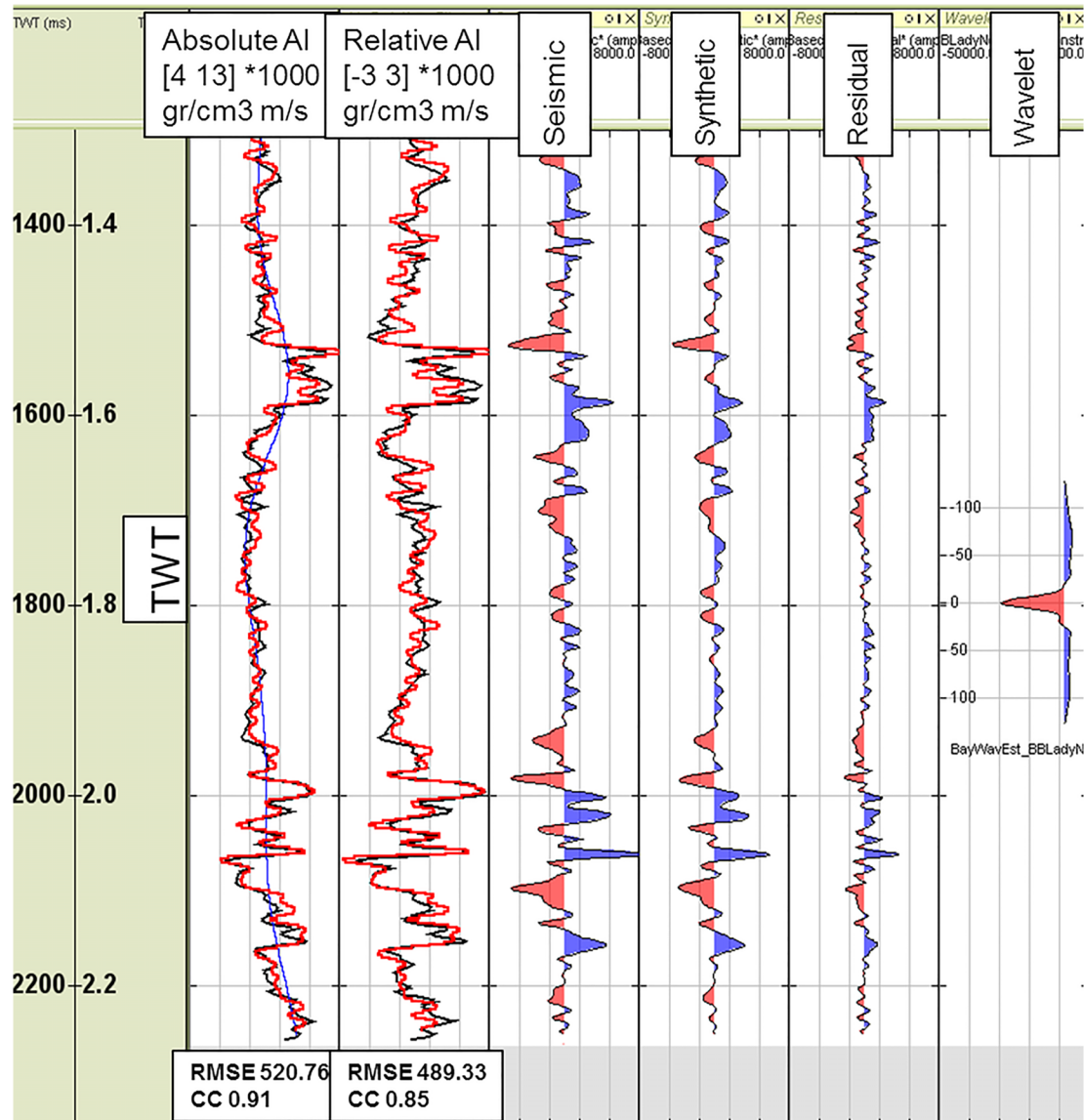


Figure 11 Blind QC at well 1 using the Bayesian time-domain least-squares wavelet with broadband priors from well 2 (see also Figure 8c). The red curve is the inverted impedance, and the black curve is the well-log impedance.

limited to the three best options found from well-tie analysis at well 1, namely constant phase, frequency-domain Papoulis with low frequency modification using the multi-taper counterpart, and Bayesian time-domain least squares with broadband priors.

Figures 8(a), (b) and (c) show well-tie plots from the three methods. Inspection of the RMSE, CC, PEP, and phase error values show that this tie is not as close as the tie at well 1, although it is still a good tie. Again, all three methods perform consistently and give similar results.

Figures 9, 10, and 11 show the blind QC at well 1. Again, all three methods perform almost equally well. The Bayesian time-domain least squares give slightly improved results in the well-tie plot of Fig. 8(c) and the corresponding blind QC in Fig. 11. This could indicate that, for shorter log lengths, the Bayesian time-domain method with broadband priors can achieve better results.

Overall, the simplicity of the constant phase wavelet and its robust performance on the cross-validation QC encourages one to choose it for this case study. That is largely due to the

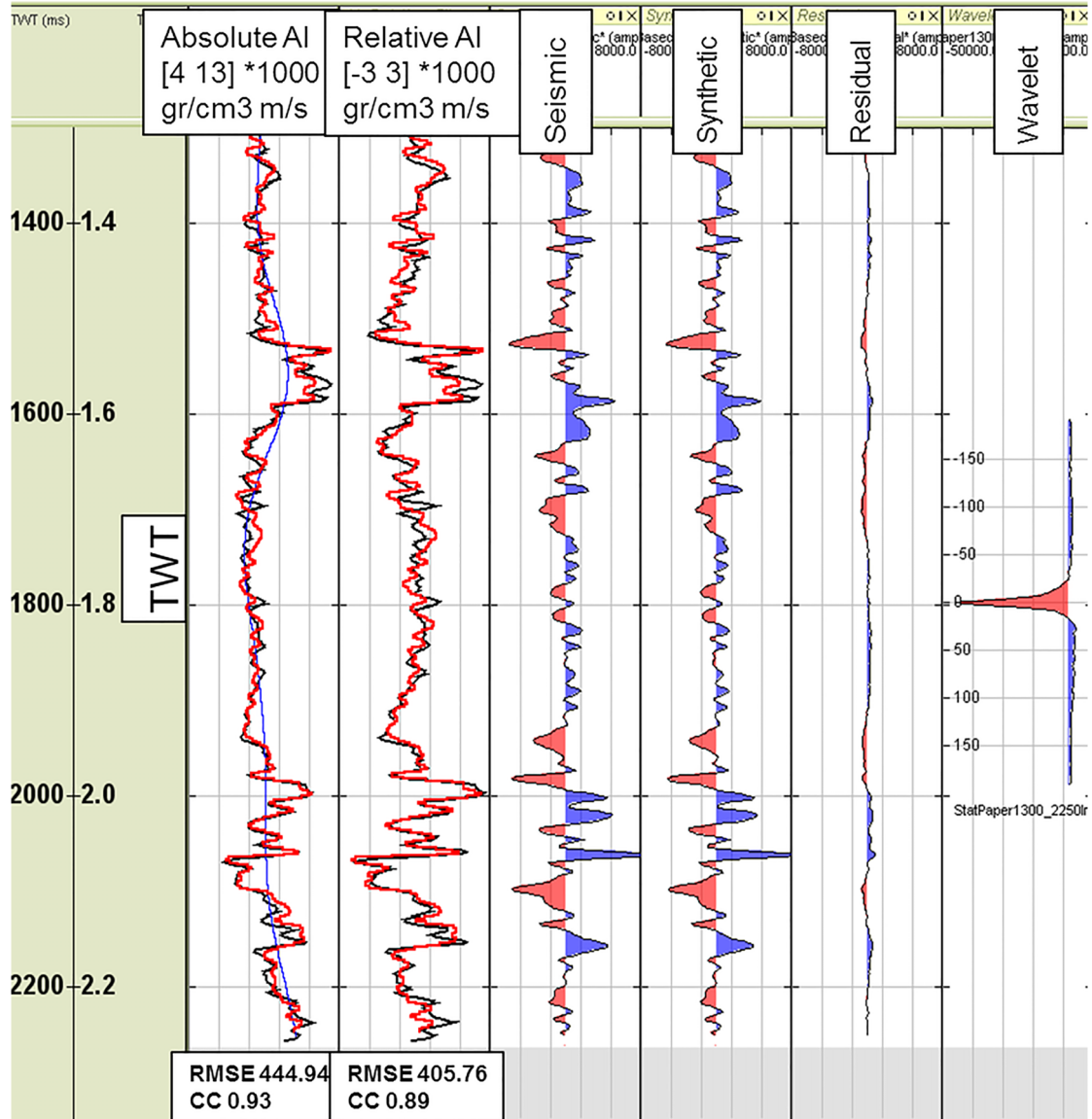


Figure 12 QC at well 1 using the constant phase wavelet estimated from well 1 (see also Fig. 1). The red curve is the inverted impedance, and the black curve is the well-log impedance.

high-quality seismic data that have been nicely processed to 180° phase with a residual phase error of only around 10°. The availability of well-conditioned logs is another reason for the good-quality well tie in this study.

3.3 Final remarks

The cross-validation or blind QC approach proposed in this paper is recommended as a powerful consistency test of the estimated wavelet across the survey at different well locations.

If one chooses to QC the wavelet only at the well location where the wavelet was estimated from, it is almost certain that the result is as good as or better than the blind QC. For instance, the constant phase wavelet estimated from well 1 in Fig. 1 performs nicely in the blind QC examples provided in this paper. Figure 12 shows the QC at well 1 instead, which as expected has a superior performance when compared with the blind QC at well 2 (e.g., Fig. 9).

The notable success of the constant-phase method observed in this application does not imply that a comparably

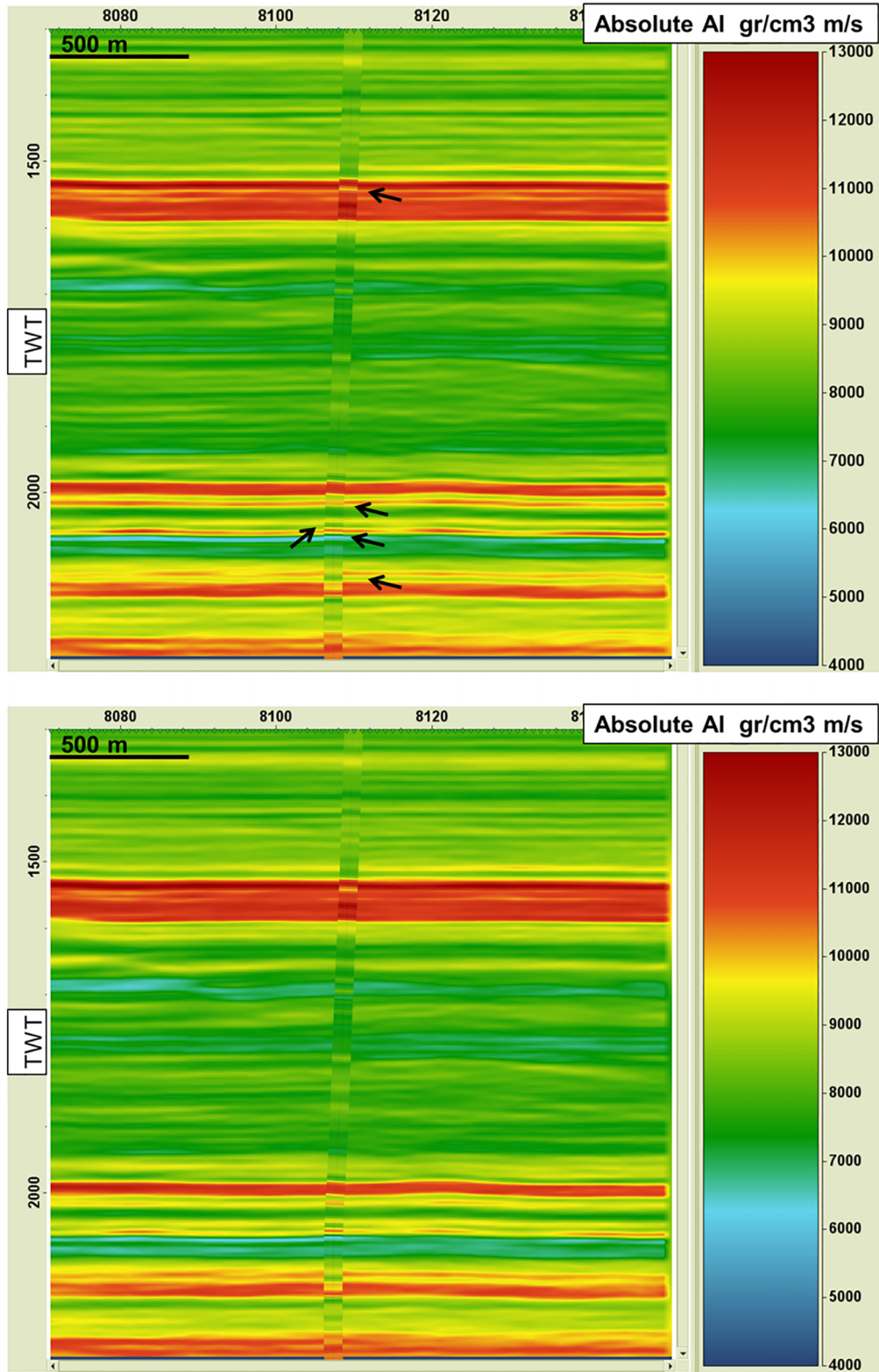


Figure 13 Section displays of inverted AI around well 1, using the wavelet of Fig. 1 (top), and a simple 180° autocorrelation wavelet for comparison Fig. 1. (bottom). Note the improvement at locations shown with arrows.

simple 0/180 phase or autocorrelation-wavelet approach will work equally well. The 10° phase difference is significant. Figure 13 shows two section displays of inverted AI around well 1, using the wavelet of Fig. 1, and a simple 180° autocorrelation wavelet for comparison. The constant phase wavelet results in a much better match, resolving thin layers unseen by the auto-correlation wavelet (see black arrows in Fig. 13).

4 CONCLUSION

Three wavelet estimation methods for broadband seismic data have been proposed and tested on a case study from the North West Shelf of Australia. The constant phase method reduces the number of degrees of freedom of the solution and splits the problem into two problems: the amplitude spectrum is estimated using multi-tapering over a long window of seismic data; the phase, time lag, and a scale factor are computed using the cross-covariance of the seismic data and the synthetic seismogram. Frequency-domain least squares does not benefit much from incorporating multi-tapering when calculating the auto- and cross-spectra. Any improvement at low frequencies is limited by the available log length. The ability to compute the errors for the wavelet's amplitude and phase spectra still gives this technique a role as a diagnostic tool, for example, in deciding whether the phase varies with frequency. In the Bayesian time-domain method, the use of broadband priors was shown to improve its performance. A cross-validation approach was demonstrated as a robust method of quality control of the estimated wavelets. The well tie used to test these techniques was a very close one. The seismic data appear to have been processed to approximately 180° phase, which made the constant phase method a valid choice. The other two methods also performed well. The application of Bayesian broadband priors, which constrain the wavelet to have a low-order polynomial spectral decay to DC, imparts smooth broadband side lobes to the wavelet and counteracts the restriction of short log lengths very effectively. A recommended work flow for general use would be to run the constant phase method prior the other two in order to understand the well tie and its potential challenges. Any improvement from the other two methods can then be judged against this.

ACKNOWLEDGEMENTS

The authors thank Ikon Science for permission to publish this work and Woodside and partners for permission to show the

real data example. Suggestions from several reviewers and the associate editor are also gratefully acknowledged. We also thank Woodside, ExxonMobil, Murphy, and VNG for sponsoring this research.

REFERENCES

- Baeten G., De Maag J.W., Plessix R.-E., Klaassen R., Qureshi T., Kleemeyer M. *et al.* 2013. The use of low frequencies in a full-waveform inversion and impedance inversion land seismic case study. *Geophysical Prospecting* **61**(4), 701–711.
- Brandt S. 1976. *Statistical and Computational Methods in Data Analysis*. North Holland Publishing.
- Denison D.G.T., Holmes C.C., Mallick B.K. and Smith A.F.M. 2002. *Bayesian Methods for Nonlinear Classification and Regression*. John Wiley & Sons.
- Deutsch C.V. and Journel A.G. 1997. *GSLIB - Geostatistical Software Library and User's Guide*. Oxford University Press.
- Douma J. and Zabihi Naeini E. 2014. Application of image-guided interpolation to build low frequency background model prior to inversion. *76th EAGE Conference and Exhibition*, Amsterdam, The Netherlands, Extended Abstracts, We G106 05.
- Gunning J. and Glinsky M. 2006. WaveletExtractor: A Bayesian well-tie and wavelet extraction program. *Computers and Geosciences* **32**, 681–695.
- Hamon B.V. and Hannon E.J. 1974. Spectral estimation of time delay for dispersive and non-dispersive systems. *Applied Statistics* **23**, 134–142.
- Jolley L.W.B. 1961. *Summation of Series*. Dover Publications Inc.
- Nielsen A.K., Klemm H. and Cherrett A.J. 2015. Joint well-tie and wavelet extraction in the impedance domain. *77th EAGE Conference and Exhibition*, Madrid, Spain, Extended Abstracts, Th N102 11.
- Papoulis A. 1973. Minimum bias windows for high resolution spectral estimates. *IEEE Transaction on Information Theory* **19**(1), 9–12.
- Poole G., Davison C., Deeds J., Davies K. and Hampson G. 2013. Shot-to-shot directional signature using near-field hydrophone data. 83rd SEG Meeting, Houston, USA, Extended Abstracts, 4236–4240.
- Riedel K.S. and Sidorenko A. 1995. Minimum bias multiple taper spectral estimation. *IEEE Transactions on Signal Processing* **43**(1), 188–195.
- Reiser C., Bird T. and Whaley M. 2015. Reservoir property estimation using dual-sensor seismic data—a case study from the West of Shetlands, UKCS. *First Break* **33**(10), 93–101.
- ten Kroode F., Bergler S., Corsten C., de Mag J.W., Strijbos F. and Tijhof H. 2013. Broadband seismic data—the importance of low frequencies. *Geophysics* **78**(2), WA3–WA14.
- Thomson D.J. 1982. Spectrum estimation and harmonic analysis. *Proceedings of the IEEE* **70**, 1055–1096.
- Walden A. and White R. 1998. Seismic wavelet estimation: a frequency domain solution to a geophysical noisy input–output problem. *IEEE Transactions on Geoscience and Remote Sensing* **36**(1), 287–297.

- White R.E. 1980. Partial coherence matching of synthetic seismograms with seismic traces. *Geophysical Prospecting* 28, 333–358.
- White R.E. 1984. Signal and noise estimation from seismic reflection data using spectral coherence methods. *Proceedings of the IEEE* 72(10), 1340–1356.
- White R.E. and Simm R. 2003. Tutorial: good practice in well ties. *First Break* 21(10), 75–83.
- White R.E. and Zabihi Naeini E. 2014. Broad-band well tie. 76th EAGE Conference and Exhibition, Amsterdam, The Netherlands, Extended Abstracts, Tu EL12 10.
- Zabihi Naeini E. 2014. Quantitative interpretation of broadband seismic data – challenges and solutions. 2nd EAGE/SBGf workshop, Rio, Brazil, Expanded Abstracts, We E06.
- Zabihi Naeini E. and Hale D. 2015. Image- and horizon-guided interpolation. *Geophysics* 80(3), V47–V56.

APPENDIX

Estimation of a phase and time lag from a cross-correlation implies the following phase law:

$$\theta(f) = 2\pi f\tau + \theta_0 + e(f), \quad (\text{A.1})$$

where f is the frequency, τ the time lag, θ_0 the phase intercept at zero frequency and $e(f)$ an error term arising from random noise. Given any parametric phase relation $\theta(f)$, Hamon and Hannon (1974) give a general equation for the variance–covariance matrix of the maximum-likelihood parametric phase estimates. This matrix is $T^{-1}\mathbf{V}^{-1}$, where T is the duration of data segments, and the (j, k) th element of the matrix \mathbf{V} is

$$v_{j,k} = 2b \sum_B \frac{\theta_j(f_l)\theta_k(f_l)}{(\gamma(f)^{-2} - 1)}, \quad (\text{A.2})$$

where $\theta_j(f_l)$ is the differential of $\theta(f)$ with respect to the j th parameter evaluated at frequency f_l using the estimated parameters, b is the analysis bandwidth of the spectral window,

B is the spectral bandwidth of the seismic data, and $\gamma(f)$ is the spectral coherence at frequency f .

This equation is not particularly informative, but it can be simplified for the parametric phase of equation (A.1). If it is further assumed that the signal-to-noise ratios and hence the spectral coherence of the recordings are fairly constant over the signal bandwidth ($\gamma(f)$ would be equivalent to the magnitude of the peak of the envelope of the cross-correlation coefficient R), then equation (A.2) becomes more revealing. In this case, the denominator can be taken outside the sums. Application of equation (A.2) requires the coherence estimates to be independent, which in turn requires that the frequencies f are separated by the analysis bandwidth b . There are therefore B/b terms in each sum. On substituting the differentials, the cross term $v_{12} = v_{21}$ contains a sum over equispaced frequencies and the diagonal term corresponding to τ has a sum over squared frequencies. The first sum is proportional to the average or centre frequency of the signal bandwidth, and the second sum can be evaluated using series (19) and (32) in Jolley (1961). Finally, inverting the matrix \mathbf{V} , we find that the variance of estimated time shift is

$$\text{variance}\{\tau\} = \frac{3}{\pi^2(B^2 - b^2)} \frac{(R^{-2} - 1)}{2BT}. \quad (\text{A.3})$$

The variance of the predicted phase shift at frequency f is

$$\text{variance}\{\theta(f)\} = \left[1 + \frac{12(f - \bar{f})}{(B^2 - b^2)} \right] \frac{(R^{-2} - 1)}{2BT}, \quad (\text{A.4})$$

where \bar{f} is the centre frequency of the signal bandwidth. Since $B^2 \gg b^2$, equation (A.3) leads to equation (4). Moreover, the phase error around the centre frequency (i.e., $f = \bar{f}$) is a better indication of the phase error in a seismic wavelet; hence, equation (A.4) leads to equation (5).